

# ZrOsSi: A $Z_2$ topological metal with a superconducting ground state

Sudeep Kumar Ghosh<sup>1</sup>, Bin Li<sup>2</sup>, Chunqiang Xu<sup>3,4</sup>, Adrian D. Hillier<sup>5</sup>,  
Pabitra K. Biswas<sup>5</sup>, Xiaofeng Xu<sup>3\*</sup> and Toni Shiroka<sup>6,7\*</sup>

<sup>1</sup>Department of Physics, Indian Institute of Technology, Kanpur 208016, India

<sup>2</sup>Information Physics Research Center, Nanjing University of Posts and Telecommunications, Nanjing 210023, China

<sup>3</sup>Key Laboratory of Quantum Precision Measurement of Zhejiang Province, Department of Applied Physics, Zhejiang University of Technology, Hangzhou 310023, China

<sup>4</sup>School of Physical Science and Technology, Ningbo University, Ningbo 315211, China

<sup>5</sup>ISIS Pulsed Neutron and Muon Source, STFC Rutherford Appleton Laboratory, Harwell Campus, Didcot, Oxfordshire OX11 0QX, United Kingdom

<sup>6</sup>Laboratory for Muon Spectroscopy, Paul Scherrer Institut, CH-5232 Villigen PSI, Switzerland

<sup>7</sup>Laboratorium für Festkörperphysik, ETH Zürich, CH-8093 Zurich, Switzerland

Correspondence\*:

X. Xu and T. Shiroka

xuxiaofeng@zjut.edu.cn, tshiroka@phys.ethz.ch

## ABSTRACT

The silicide superconductors (Ta, Nb, Zr)OsSi are among the best candidate materials for investigating the interplay of topological order and superconductivity. Here, we investigate in detail the normal-state topological properties of (Ta, Nb, Zr)OsSi, focusing on ZrOsSi, by employing a combination of <sup>29</sup>Si nuclear magnetic resonance (NMR) measurements and first-principles band-structure calculations. We show that, while (Ta, Nb)OsSi behave as almost ideal metals, characterized by weak electronic correlations and a relatively low density of states, the replacement of Ta (or Nb) with Zr expands the crystal lattice and shifts ZrOsSi towards an insulator. Our *ab initio* calculations indicate that ZrOsSi is a  $Z_2$  topological metal with clear surface Dirac cones and properties similar to a doped strong topological insulator.

**Keywords:** Topological metals, superconductivity, ab-initio calculations, surface states, NMR

## 1 INTRODUCTION

Topological metals (TMs) are special metallic materials characterized by a nontrivial topology, in particular, by their topologically-protected surface states [1, 2]. Depending on the presence of a “gap” at the Fermi level of their electronic band structure, they are broadly classified into two categories. (i) TMs with a continuous *direct band gap* over all the  $k$ -points of the Brillouin zone, which exhibit also a nontrivial  $Z_2$  topological invariant, are called  $Z_2$  TMs [3, 4]. (ii) TMs with topologically nontrivial *band crossings* near the Fermi level are called nodal semimetals. In turn, according to the dimensionality of the nodes,

nodal semimetals are further classified into nodal-point, nodal-line and nodal-surface semimetals [1, 2]. Due to their novel quantum properties, that are of interest to both fundamental physics and technological applications [1, 2], TMs have been at the forefront of research on quantum materials.

Owing to their nontrivial band topology and the associated rich physical properties, TMs represent unique platforms for investigating the interplay between topology, strong correlation and superconductivity. In this regard, superconducting TMs are of particular interest. For instance, unconventional superconductivity with time-reversal symmetry (TRS) breaking [5] was recently discovered in the Weyl nodal-line semimetals La(Pt, Ni)Si and LaPtGe [6] and in the Dirac semimetal LaNiGa<sub>2</sub> [7, 8]. In particular, the recently discovered superconducting  $Z_2$  TMs (Cs, Rb, K)V<sub>3</sub>Sb<sub>5</sub> with a layered kagome crystal structure have generated a lot of interest in the community [9, 10]. However, due to the inherent geometric frustration, typical of the kagome lattice, these materials exhibit several competing orders. While their interplay leads to new and interesting phenomena [9, 10], at the same time it becomes difficult to grasp the underlying physics of the different phases.

In this respect, the silicide superconductors (Ta, Nb)OsSi are special since, despite being nonsymmorphic symmetry-protected semimetals [11, 12, 13, 14] (with time-reversal symmetry-breaking superconducting ground states), their crystal structure does not have any geometric frustration. ZrOsSi, which is isostructural with (Ta, Nb)OsSi, is also superconducting, but with a superconducting transition temperature  $T_c \sim 1.7$  K [15] much lower than that of TaOsSi (5.5 K) and NbOsSi (3.1 K). This hints that possibly the physics of ZrOsSi is qualitatively different from that of its isostructural counterparts (Ta, Nb)OsSi, including some remarkably different topological properties. Motivated by these possibilities and by recent developments regarding topological metals, in this article, we investigate in detail the normal-state properties of ZrOsSi and contrast them with those of (Ta, Nb)OsSi.

Spin-orbit coupling (SOC) is a fundamental property of the electron motion, which lifts the spin degeneracy and renormalizes energy bands. Most importantly, it can lead to band inversions, which is the key to the physics of topological insulators and helical spin textures, as well as of their surface states [16]. Consequently, in quantum materials, SOC effects lie at the heart of topological properties and of phenomena related to the Berry curvature, such as quantum spin Hall effect [17], topological insulators [16], and Majorana fermions [18]. Since SOC grows larger in heavier elements, it typically does not play a role in  $3d$  systems, but it becomes important in  $4d$ ,  $5d$  and  $5f$  systems [19]. In view of this, we devote special attention to SOC effects and their possible influence on the topological character of ZrOsSi.

Nuclear magnetic resonance (NMR) is a powerful bulk probe, which provides local resolution of the electronic properties, also in the case of topological materials [20]. Thus, modifications in the electronic band structure due to SOC can influence the nuclear magnetic shielding and, hence, be detected by NMR from the corresponding NMR frequency shift [20, 21, 22, 23]. Further, in topological materials, the coherence time of nuclear spins is often reduced by their coupling to the surface states [24]. Hence, NMR can be used to probe both the surface metallic states and the bulk electronic structures [25, 21, 22, 26]. For instance, in large surface-to-volume samples, NMR has been successfully employed to detect and characterize nuclei in the proximity of the topologically protected surface states [27, 28, 29]. While an identification of the nuclei near the surface has been achieved in nanopowdered samples, a general characterization of the electronic surface states using NMR remains difficult. Nevertheless, NMR has been used to investigate the physical properties of surface metallic states in some semiconductor-based bulk- or low-dimensional systems [30, 31].

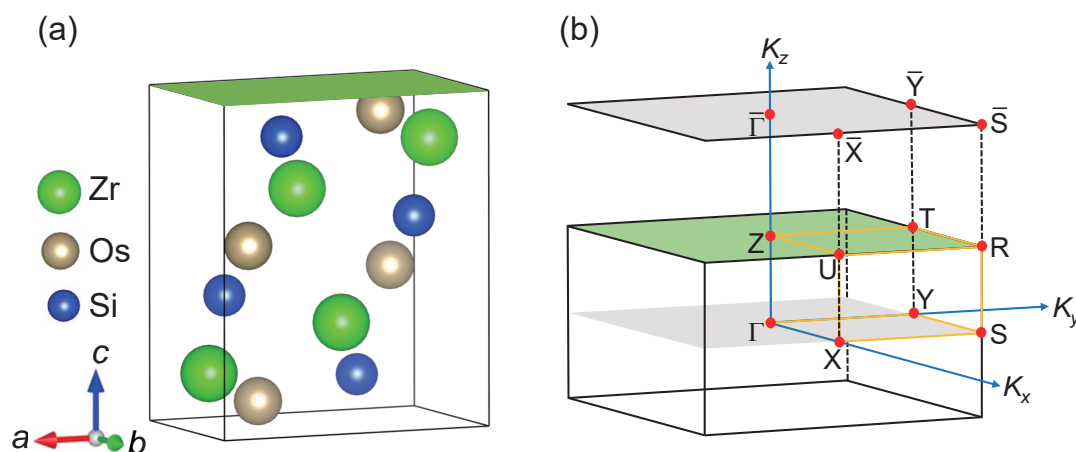


**Figure 1. Crystal structure of ZrOsSi.** (a) Unit cell of the centrosymmetric orthorhombic crystal structure. (b) First Brillouin zone, including the (001) surface-Brillouin zone and the high symmetry directions. The termination point of the slab calculation is indicated by the green-colored plane.

Recently, the combination of NMR and first principles band structure calculations has been used as a powerful tool to determine the topology of several quantum materials [32, 33, 22, 34]. For instance, NMR shift measurements in  $\text{ZrTe}_5$  provide signatures of a topological phase transition and of band inversion [32]. Further, in  $\text{Bi}_2(\text{Se}, \text{Te})_3$ ,  $^{209}\text{Bi}$  NMR could show that its band inversion results from a charge redistribution between different crystal sites, in quantitative agreement with DFT calculations [33, 22]. Inspired by these examples, here we investigate the topological properties of ZrOsSi by combining band-structure calculations with NMR measurements. Using detailed first-principles calculations we show that ZrOsSi is a  $Z_2$  topological metal with physical properties similar to a doped strong topological insulator [35]. This conclusion is further corroborated by our extensive NMR measurements, which clearly show that, while (Ta, Nb)OsSi are good metals, ZrOsSi exhibits distinct semimetallic features.

## 2 RESULTS

Polycrystalline samples of (Ta, Nb, Zr)OsSi were synthesized via the arc-melting method [15, 36, 14]. 99.99% pure tantalum (niobium or zirconium) pellets, osmium ingots, and silicon pieces, all from Alfa Aesar, were used as starting materials. After preparing them in the prescribed 1:1:1 molar ratio, the reagents were inserted into an arc furnace, which was purged multiple times and eventually filled with pure argon. The as-cast ingots were remelted more than ten times to ensure phase homogeneity. Finally the ingots were sealed under vacuum in a quartz tube and annealed at 1273 K for nine days. In the whole process, the specimens lost very little weight (less than 1%) due to the non-volatile nature of the reactants. This ensured that the stoichiometry of the as-grown samples matched the nominal one. Note that, due to the toxicity of Os, it is generally difficult to grow Os-based materials, as they require special handling. The obtained (Ta, Nb, Zr)OsSi samples crystallize in a centrosymmetric orthorhombic  $\text{TiNiSi}$ -type structure, with space group  $Pnma$  (No. 62) [15, 36, 14]. The crystal structure of ZrOsSi and its corresponding Brillouin zone are shown in Fig. 1. For the basic characterization of all the materials, we refer to our previous work [36, 14].

### 2.1 Electronic band structure

The electronic band structure of ZrOsSi was computed by first-principles calculations based on density functional theory using the full-potential linearized augmented plane wave (FP-LAPW) method, as implemented in the WIEN2k program suite [37]. Here, we use the exchange-correlation potential from the

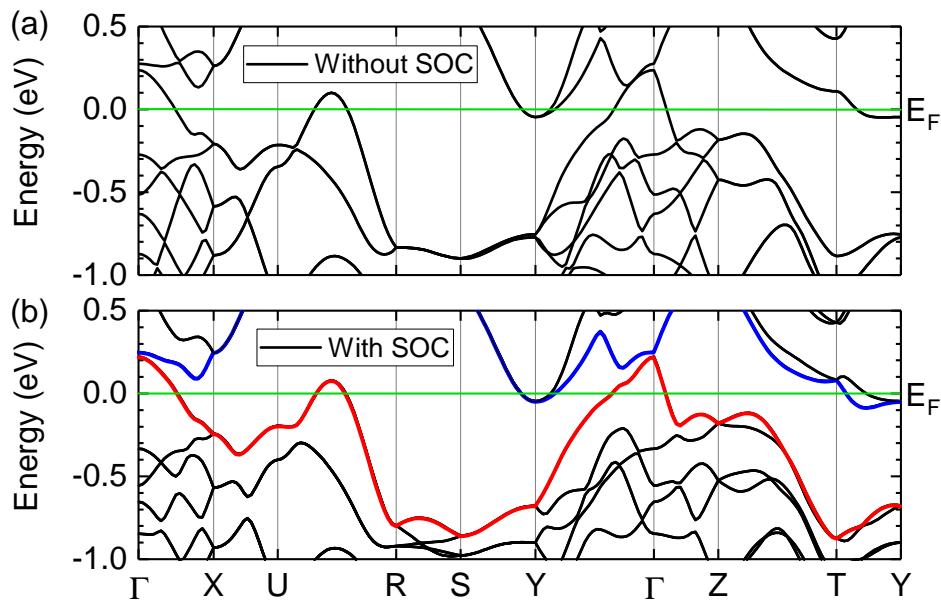


**Figure 2. Electronic band structure of ZrOsSi:** (a) without SOC and (b) with SOC. In (b), the highest occupied “valence” band and the lowest “conduction” band are marked in red and blue, respectively.

generalized gradient approximation (GGA) [38], with the plane-wave cutoff being defined by the condition  $rk_{\max} = 7.0$ , with  $r$  being the minimum LAPW sphere radius and  $k_{\max}$  being the plane-wave-vector cutoff. For ZrOsSi, the lattice parameters, optimized using DFT, are:  $a = 6.43(9) \text{ \AA}$ ,  $b = 4.08(0) \text{ \AA}$ , and  $c = 7.50(7) \text{ \AA}$ , consistent with previous reports [15]. The Wyckoff positions corresponding to the structure of ZrOsSi are: Zr  $4c$  (0.01253, 0.25, 0.81533), Si  $4c$  (0.21227, 0.75, 0.62165), Os  $4c$  (0.16157, 0.25, 0.44187). The lattice parameters for TaOsSi [14] are:  $a = 6.26(5) \text{ \AA}$ ,  $b = 3.89(3) \text{ \AA}$ , and  $c = 7.25(9) \text{ \AA}$ ; and for NbOsSi [14] are:  $a = 6.28(1) \text{ \AA}$ ,  $b = 3.89(7) \text{ \AA}$ , and  $c = 7.27(3) \text{ \AA}$ . Clearly, replacing Ta or Nb in (Ta, Nb)OsSi by Zr leads to an expansion of the unit cell.

The electronic band structure of ZrOsSi, with and without considering the effects of SOC, are shown in Fig. 2(a) and Fig. 2(b), respectively. We note that several bands cross the Fermi level, leading to the electron- and hole Fermi surfaces shown in Fig. 3 (without SOC). Inside the Brillouin zone, one can identify extended regions where several Fermi-surface sheets are parallel and close to each other. This feature is also present in the Fermi surfaces of (Ta, Nb)OsSi, where it was argued to influence the nature of their superconducting ground states [14]. The reason for the closeness of the different Fermi surface sheets and the relatively small sizes of the Fermi surfaces of (Ta, Nb, Zr)OsSi can be traced back again to the nonsymmorphic symmetries of these materials, similar to that of others with the same space-group symmetry [13, 39].

From Fig. 2, we note that SOC causes a significant band splitting. In particular, it results in a maximum band-splitting of  $\sim 100 \text{ meV}$  along the  $TY$  direction, where an extra Fermi-surface sheet emerges due to SOC. Most importantly, from Fig. 2(b), we note that due to SOC there is a continuous direct energy gap throughout the Brillouin zone between the highest occupied “valence” band (shown in red) and the lowest unoccupied “conduction” band (shown in blue). As a result, ZrOsSi can be thought of as a semimetal, for which the classification of band insulators in three dimensions (3D), based on the  $Z_2$  topological invariants ( $\nu_0; \nu_1\nu_2\nu_3$ ), is also applicable [40]. From the topological point of view, such identification is possible since its bands can be continuously deformed into those of an insulating system, characterized by a full gap throughout the Brillouin zone. In general, the  $Z_2$  topological invariants can be computed by calculating

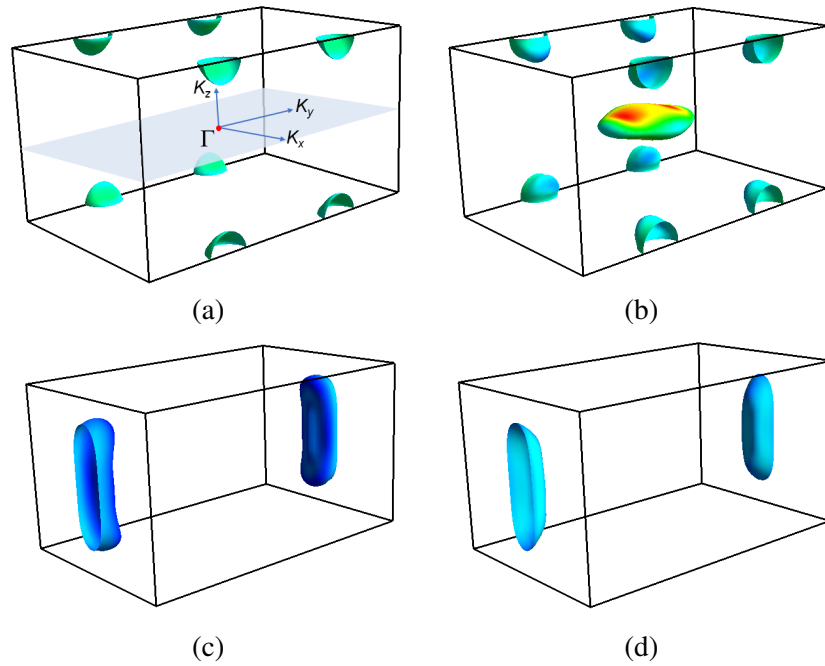


**Figure 3. Fermi surfaces of ZrOsSi without SOC.** The four Fermi-surface sheets are shown in (a), (b), (c) and (d). Note that between the Fermi surfaces shown in (a) and (b) and those in (c) and (d) there are several regions where two of the Fermi-surface sheets are parallel and close to each other. The color map denotes Fermi velocity.

the evolution of the Wannier charge centers (WCCs) for the six time-reversal invariant planes:  $k_x = 0, \pi$ ;  $k_y = 0, \pi$ ; and  $k_z = 0, \pi$  [41, 42] as shown in Fig. 4. In the ZrOsSi case, the  $Z_2$  invariants are 1 for the  $k_x = 0, k_y = 0$ , and  $k_z = 0$  planes, and 0 for the  $k_x = \pi, k_y = \pi$ , and  $k_z = \pi$  planes. This implies that, in ZrOsSi, the  $Z_2$  topological invariants are (1; 000), thus indicating that ZrOsSi is a *strong topological material*.

Since ZrOsSi has a centrosymmetric structure, we can confirm the above classification scheme by computing the  $Z_2$  topological invariants from the product of the parity eigenvalues of the filled valence bands (up to the red band in Fig. 2(b)) at the eight time-reversal invariant momentum (TRIM) points [40] with SOC. These parity products up to the red band in Fig. 2(b) are  $-1$  at the  $\Gamma$  point and  $+1$  at all the other TRIM points. This leads to the  $Z_2$  topological invariants (1; 000) for ZrOsSi, the same as those obtained by the WCC method described above. As a result, we conclude that ZrOsSi is a  $Z_2$  topological metal, which can be continuously deformed into a strong  $Z_2$  topological insulator. In this sense, the physics of ZrOsSi is expected to be similar to that of a doped topological insulator [35].

We show the orbital-decomposed band structure of ZrOsSi in Fig. 5, where the  $p$ - $d$  band inversions along the  $\Gamma - X$ ,  $\Gamma - Y$ , and  $\Gamma - Z$  directions are clearly visible, thus supporting our identification of ZrOsSi with a strong topological material. Due to the bulk-boundary correspondence, there will be topologically protected metallic surface states in ZrOsSi. We investigate the surface states by computing the surface spectral function or the surface-state spectrum using surface Green's function and maximum localized Wannier functions, as implemented in the WannierTools package [42]. In ZrOsSi, we compute the surface-state spectrum for a (001) slab, as well as the spectral function for the corresponding bulk. In both cases, we consider the SOC effects. The bulk spectral function is shown in Fig. 6(a) and the corresponding surface-state spectral function for the slab is shown in Fig. 6(b) on the (001) surface Brillouin zone. For

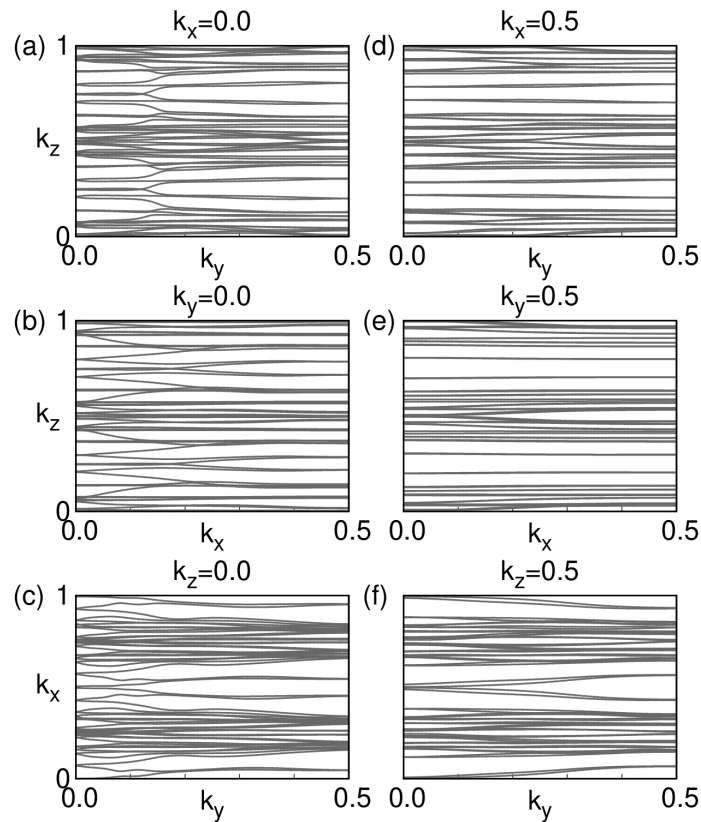


**Figure 4. Wannier charge centres for ZrOsSi.** The evolution of the Wannier charge centers in the six different time-reversal invariant planes is shown in the panels (a) - (f).

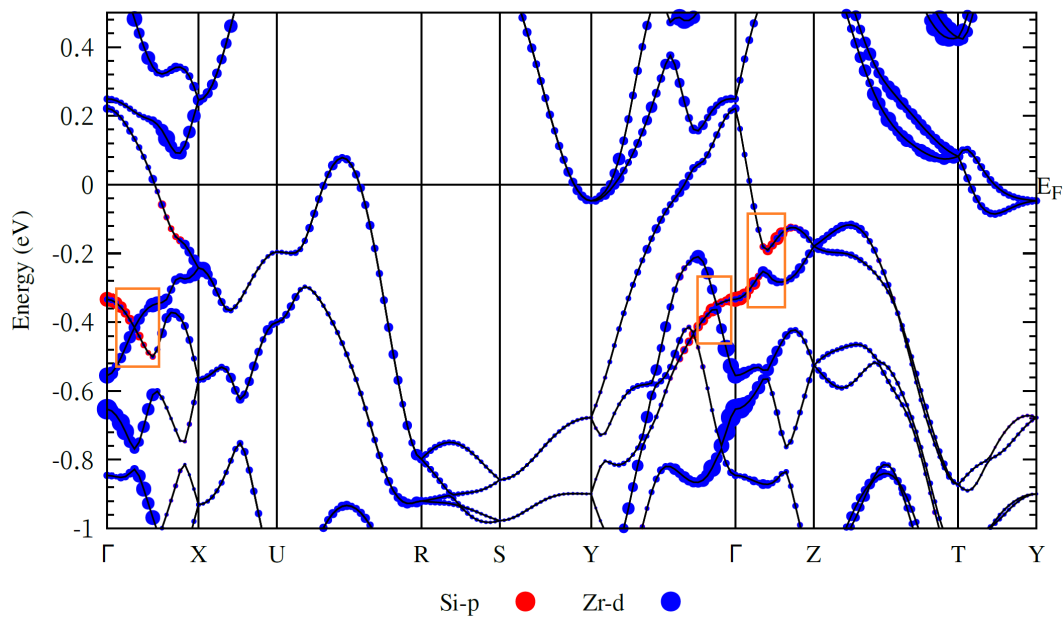


**Figure 5. Orbital-resolved band structure of ZrOsSi.** The Si-*p* orbitals are marked in red and the Zr-*d* orbitals are marked in blue. The orange boxes highlight the regions where band inversion occurs between the Si-*p* and Zr-*d* bands.

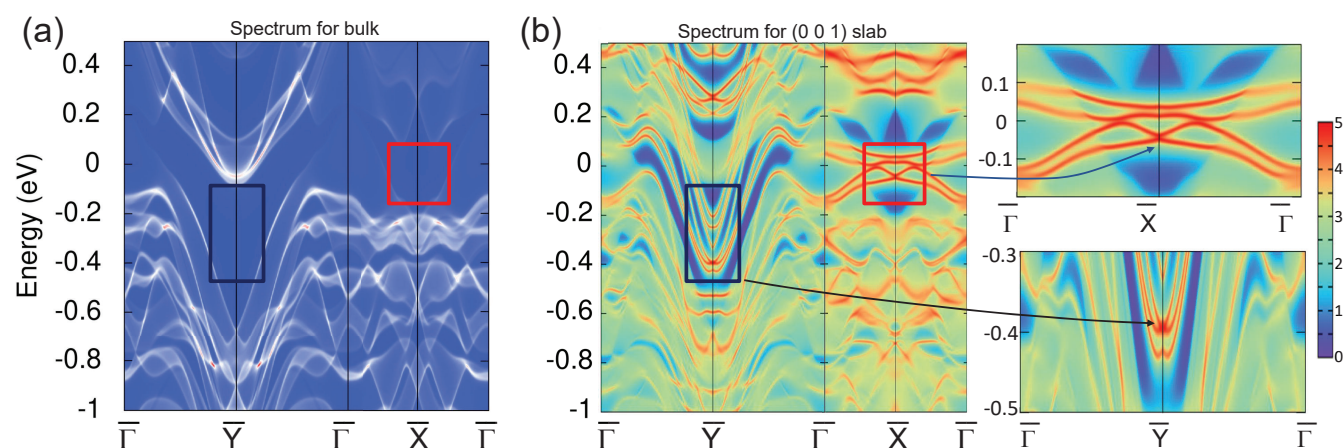


**Figure 6. Surface states for ZrOsSi.** The surface-state spectrum of ZrOsSi on the (001) surface Brillouin zone along the  $\bar{\Gamma} - \bar{X} - \bar{\Gamma}$  and  $\bar{\Gamma} - \bar{Y} - \bar{\Gamma}$  high-symmetry directions when including SOC. The spectral function for the bulk in (a) and for a slab with (001) surface in (b) are shown. Zoomed plots of the marked regions in (b) are shown in the rightmost panels. The color map denotes Fermi velocity.

clarity, here we focus on the high-symmetry  $\bar{\Gamma} - \bar{X}$  and  $\bar{\Gamma} - \bar{Y}$  directions (motivated also by the evidence of band inversion along these directions, as shown in Fig. 5).

Some key regions where the surface states are clearly visible are marked in Fig. 6(b), where we show also their zoomed versions. Note that, while in these regions the spectral function is nonzero for the slab, it is zero for the bulk [see Fig. 6(a)]. This fact, together with the existence of nontrivial topological invariants and of band inversions described above, clearly indicate that, in ZrOsSi, the surface states are indeed due to its nontrivial bulk topology. The apparent asymmetry of the surface-state spectrum along the two high symmetry directions in Fig. 6(b) is due to the direct gap moving up and down in energy, depending on the direction away from the  $\Gamma$  point, as shown in Fig. 2(b). We note that, just below the Fermi level, there are several topologically-protected surface Dirac cones. In our case, an odd number of them reflects the odd number of bulk band inversions, thus confirming the  $Z_2$  topological-metal nature [3] of ZrOsSi, as highlighted by the zoomed images in the rightmost panels in Fig. 6(b). The surface states relevant to our discussion are most evident at  $\sim 0.05$  eV below the Fermi level, at the  $\bar{X}$  point, and at  $\sim 0.4$  eV below the Fermi level, at the  $\bar{Y}$  point. Hence, the normal state of ZrOsSi, which is like a strong topological insulator, is *qualitatively different* from that of its isostructural counterparts (Ta,Nb)OsSi, which are nonsymmorphic symmetry-protected semimetals [11, 12, 13, 14]. The basic difference between insulating and metallic character of these materials can be probed, for instance, by NMR experiments. Therefore, in the following section, we report about and discuss our systematic investigation of these materials using NMR.

## 2.2 $^{29}\text{Si}$ NMR: ZrOsSi vs. TaOsSi and NbOsSi

NMR investigations of AOsSi ( $A = \text{Ta, Nb}$  and  $\text{Zr}$ ) are, in principle, very suitable, considering the presence of three NMR-active nuclei:  $A$ , Os and Si. However, the large spin and/or quadrupole moments of  $^{93}\text{Nb}$  and  $^{181}\text{Ta}$ , and the low-frequency, low-abundance of  $^{91}\text{Zr}$ , make the  $A$  nuclei inapt for NMR experiments. Similarly,  $^{189}\text{Os}$  has a low natural abundance and a low gyromagnetic ratio. These factors suggest the  $I = 1/2$   $^{29}\text{Si}$  nucleus as the only viable microscopic probe for a systematic study of the AOsSi series. Since the magnetic field required for the NMR experiments suppresses an already low superconducting  $T_c$  (of only  $\sim 1.7$  K in the ZrOsSi case [15]), we had to limit our investigations to the normal-state electronic properties of ZrOsSi. Yet, this is not a major limitation, since we can still investigate the consequences of

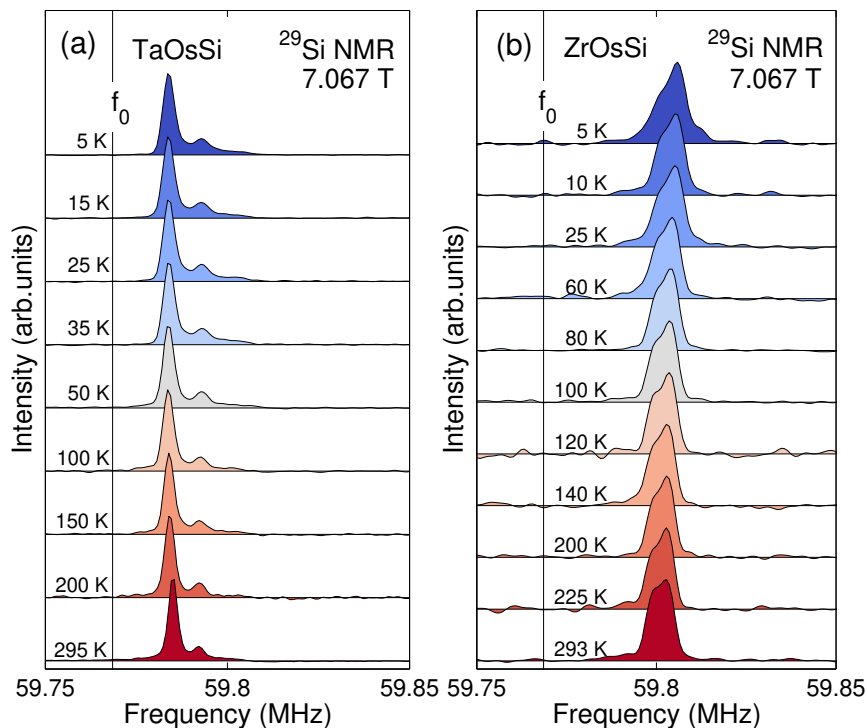


**Figure 7.**  $^{29}\text{Si}$  NMR line shapes of powder samples measured at  $\sim 7$  T in TaOsSi (a) and ZrOsSi (b). The vertical lines at  $f_0$  denote the reference Si-NMR signal. As the temperature is lowered, the lineshapes broaden and shift smoothly to higher frequencies. Note the much narrower lines and smaller shifts in TaOsSi vs. ZrOsSi, here highlighted by using the same frequency scale.

the nontrivial band topology of ZrOsSi, as compared with the conventional TaOsSi and NbOsSi metals. Note that, for  $^{29}\text{Si}$  to be an effective probe, the Si  $3p$  orbitals should contribute to the inverted bands responsible for the topological properties (here, the red band in Fig. 2). As clearly evidenced from the orbital resolved DOS shown in Fig. 5, this is indeed the case, further justifying the use of  $^{29}\text{Si}$  NMR as a probe of the topological properties of ZrOsSi.

The  $^{29}\text{Si}$  NMR spectra, collected at selected temperatures in a 7-T field, are shown in Fig. 7. Since the NMR line shapes of TaOsSi and NbOsSi are quite similar, here we compare the representative line shapes of TaOsSi in Fig. 7(a) with those of ZrOsSi in Fig. 7(b). In TaOsSi we observe a narrow main peak (at 59.785 MHz), followed by a secondary hump of negligible magnitude to the right. The latter is most likely due to impurities — probably arising from unreacted components — beyond the detection threshold of XRD. The unique crystallographic position of Si nuclei inside the  $Pnma$  structure of TaOsSi is reflected in the single main peak. Its position is almost independent of temperature and it shows only a smooth increase in width as the temperature is lowered. The shift from the  $^{29}\text{Si}$  reference frequency decreases with temperature, to saturate below 100 K. Such trends are more clearly seen in Fig. 8, where the evolution of both shifts and widths with temperature is quite smooth. In particular, the limited increase in width as the temperature is lowered is typical of nonmagnetic materials.

Although normally silicon exhibits single narrow peaks, in ZrOsSi we observe a double NMR peak (centered at 59.8 MHz), compatible with its atomic coordination. Here, Si atoms reside in the  $4c$  sites of the orthorhombic structure shown in Fig. 1, bonded in a 10-coordinate geometry to 4-Os and 6-Zr atoms, on average 245 pm and 285 pm apart, respectively. Further, considering that Os is twice as electronegative as Zr, we expect a measurable line splitting into two groups with  $\sim 2 : 3$  ratio, as experimentally observed. This



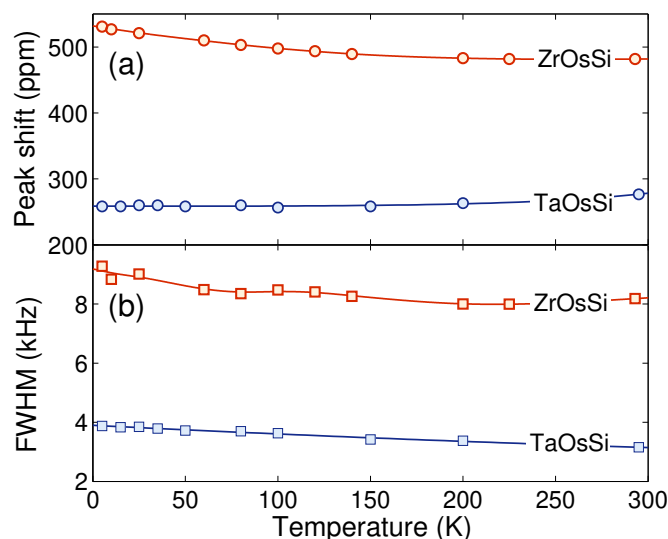


**Figure 8. Temperature dependence of (a)  $^{29}\text{Si}$  NMR line shifts and (b)  $^{29}\text{Si}$  NMR line widths for ZrOsSi and TaOsSi.** The full lines are guides to the eye. In ZrOsSi, the shift decreases by 9% in the investigated temperature range. The limited change in linewidth indicates the lack of a magnetic order. In TaOsSi, both shifts and widths are much smaller than in ZrOsSi.

assignment, however, should explain also the TaOsSi lines, since Ta and Zr have similar electronegativities and the two compounds have identical  $Pnma$  crystal structures (albeit with slightly different lattice parameters [15]). The different NMR lineshapes of TaOsSi and ZrOsSi (see Fig. 7) might instead arise from the different topological character of ZrOsSi compared to that of the standard metal TaOsSi.

This hypothesis is indirectly confirmed by previous  $^{77}\text{Se}$  NMR studies of the  $\text{Bi}_2\text{Se}_3$  topological insulator, which also shows two distinct peaks in the NMR spectra, of which the shoulder was assigned to the topologically nontrivial surface effects [28]. These results suggest that NMR may be used as a sensitive and effective probe of the nontrivial surface states in topological insulators, although a detailed theoretical backing is still missing.

As shown in Fig. 8, in the normal state, ZrOsSi exhibits a  $^{29}\text{Si}$ -NMR shift of ca. 500 ppm and a line width of ca. 8.5 kHz, both of which decrease smoothly with temperature, to saturate above 200 K. In contrast with metallic TaOsSi, where the electronic environment of Si nuclei is more homogeneous, the twofold larger line width of ZrOsSi reflects its insulating nature. In general, the total shift  $K$ , consists of an orbital- (chemical)  $K_{\text{orb}}$  and a spin part  $K_s$ . Considering the  $\sim 200$  ppm chemical shift of sixfold coordinated Si [43], the shift we observe in ZrOsSi is essentially of chemical nature ( $\sim 350$  ppm), with the spin contribution (arising from the conduction electrons) being marginal. This, too, is indicative of a poor metallic behavior, as confirmed also by electronic band-structure calculations, which indicate a deeply suppressed density of states at the Fermi level, here dominated by the Os- and Zr  $d$ -orbitals. We expect this to be reflected in very long spin-lattice relaxation times.

Indeed, this is confirmed by a comparison of the  $1/T_1$  relaxation rates of ZrOsSi with that of its isostructural counterparts NbOsSi and TaOsSi, as shown in Fig. 9. (Ta, Nb)OsSi show fast relaxation rates (even at low temperature) and a practically linear dependence of  $1/T_1$  vs.  $T$  (Fig. 9a). This is evident also from their almost constant Korringa product [44]  $1/(T_1T)$  ( $= 6.5 \times 10^{-3} \text{ s}^{-1}\text{K}^{-1}$ ), shown in Fig. 9b. The relatively small value of the Korringa product indicates a low electronic density of states at the Fermi level  $E_F$  of NbOsSi and TaOsSi, a result compatible with the electronic band-structure calculations [36], which suggest that, even in the presence of SOC, both compounds retain their metallic character. These results are

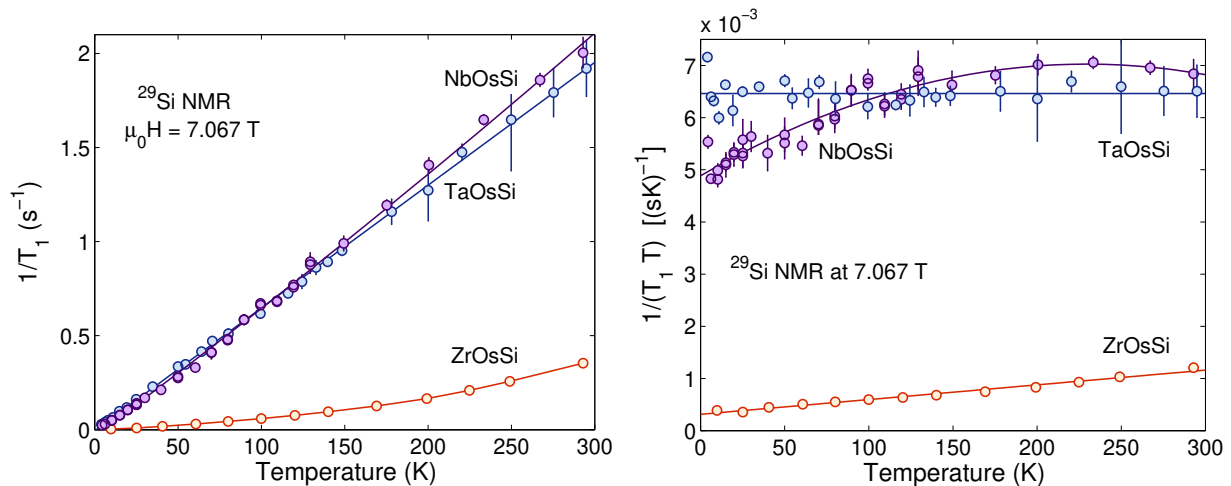


**Figure 9. Comparison of the NMR relaxation rates.** Comparison of (a)  $\frac{1}{T_1}$  and (b)  $\frac{1}{T_1 T}$  vs. temperature for ZrOsSi, NbOsSi, and TaOsSi. While the last two show a very similar (almost) linear behavior, ZrOsSi exhibits an almost quadratic dependence on  $T$ . In addition the density of states of ZrOsSi (see panel b) is a factor of ten lower, most likely reflecting its expanded lattice constants.

in stark contrast with the relaxation rates and the  $1/(T_1 T)$  product of ZrOsSi, almost an order of magnitude smaller, typical of semimetals or insulating materials.

The NMR results in the normal state of (Ta, Nb) OsSi discussed above are in agreement with the resistivity measurements [36, 14], which show that the low-temperature resistivity follows a  $T^2$ -law, i.e., these materials exhibit a good Fermi-liquid behavior. Recently, (Ta, Nb) OsSi were reported to be nonsymmorphic symmetry-protected semimetals [11, 12, 13, 14], with the SOC effects playing a crucial role in determining their topological properties. Although NMR is not a direct probe of the topological properties, the lack of any anomalous behavior in the electronic properties of (Ta, Nb) OsSi as seen by NMR is a bit surprising, since one expects to see a change in the NMR shift if SOC changes the electronic band structure [20, 21, 22, 23]. In view of the strikingly different electronic behavior of (Ta, Nb) OsSi vs. ZrOsSi (see Fig. 9), one might wonder whether SOC has some role to play, which prompts for a closer comparison of the different SOC strengths of these materials.

The calculation of SOC is not straightforward. However, thanks to the early efforts of Herman [45, 46], based on the Hartree-Fock method, as well as to more recent results (see, e.g., Fig. 1 in Ref. [47]), we have reliable estimates of SOC for all the elements. Considering the almost  $\sim Z^2$  dependence of SOC with the atomic number  $Z$ , we expect it to increase slightly from the  $4d$ -element Zr ( $Z = 40$ ) to the  $4d$ -element Nb ( $Z = 41$ ), and even more so to the  $5d$ -element Ta ( $Z = 73$ ). A similar trend is indeed found from band-structure calculations: while the SOC-induced maximum band splitting near the Fermi level is  $\sim 100$  meV in both ZrOsSi (see Fig. 2) and NbOsSi [14], it is  $\sim 140$  meV in TaOsSi [36]. We note that since both Nb and Ta belong to group-5 of the periodic table, their comparison excludes the role of valence electrons and highlights that of SOC.

However, since the experimental results in Fig. 9 show the NbOsSi and TaOsSi datasets to be basically clustered together, possibly the SOC effects are not the driving force for the observed phenomena. To justify these results we note that Zr exhibits a lower formal valency (+4), resulting in larger atomic and lattice parameters. Therefore, it does not come as a surprise that Zr acts as a lattice expander and moves the material towards the insulating side. Indeed, although the NbOsSi, TaOsSi, and ZrOsSi silicides share

the same TiNiSi-type structure (space group  $Pnma$ ,  $Z = 4$ ), ZrOsSi is very different from the other two. (i) While NbOsSi and TaOsSi have practically the same cell parameters and unit-cell volume (differing by less than 0.5%), ZrOsSi shows an 8.6% increase in unit-cell volume, with a remarkable increase in all the cell parameters ( $a \sim +1.7\%$ ,  $b \sim +3.95\%$ ,  $c \sim +2.2\%$ ). (ii) The coordinates of Si (both relative and absolute) inside the unit cell change remarkably in ZrOsSi, implying an increase of ca. 3.5% in the interatomic distances [15].

The clear conjecture, therefore, is that the replacement of Nb (or Ta) with Zr corresponds to an expansion of the crystal lattice (i.e., to a negative chemical pressure) and consequently to a significant weakening of its metallic nature. These conclusions, are in good agreement with the atomic and covalent radii [48] of Nb and Ta (both being very similar and with the same formal valence of +5), to be contrasted with the 8% larger radius of Zr (with a formal valence +4 and here acting as lattice expander).

Incidentally, the negative chemical pressure occurring in ZrOsSi complements well our previous high-pressure study of TaOsSi [36], i.e., it allows us to understand how TaOsSi would have behaved under lattice expansion. As such, it would be interesting to investigate ZrOsSi further by means of other experimental techniques.

### 3 DISCUSSION

Now we discuss critically some of our results, by comparing them with those of other topological materials. In principle, NMR is not the most suitable technique for studying topological phases of matter. Certainly, it is worth noting that while NMR is a local probe, the topological invariants however are nonlocal. Additionally, NMR primarily delves into the bulk properties, whereas topological invariants become apparent at the material's boundaries. Nonetheless, these challenges have not discouraged a multitude of experimental endeavors [20, 21, 22, 23] aimed at detecting direct or indirect signatures of topological invariants through NMR methods.

In particular, the use of nanoparticles allows for a more direct sampling of the surface states of a TI. The situation is similar to the NMR studies of superconductors which, in principle, would be very difficult, since RF fields cannot penetrate an ideal conductor. Surprisingly, with clever experiments, an ill-suited technique can still be made useful to provide the SC gap, the type of pairing, etc. [49, 50, 51].

Also in case of topological materials, the above experiments have been partly successful, although the results appear to offer conflicting responses (see, e.g., [22]). This is in part due to the lack of theoretical guidance and to the fact that calculations need to refer to the exact nucleus and compound under study. This is further complicated by the computationally difficult task of carrying DFT calculations of NMR shifts in conducting and strongly spin-orbit coupled crystals [24]. Finally, it is not easy to single out the orbital effects in NMR shifts (peculiar to each material), as opposed to the universal features expected for topological invariants. All the above facts suggest that further theoretical research is needed to enable the detection of genuine topological signatures via bulk NMR.

On the experimental side, large surface-to-volume samples (e.g. powders) are needed to detect and characterize the nuclei in the proximity of the topologically-protected surface states. While nanopowders are advantageous in this respect, their electronic band structures may be altered significantly due to quantum size effects. Consequently, standard powders (as in our case) might represent a good compromise for obtaining a suitable NMR signal from the topological phases despite a modest surface-to-volume ratio. In general, it has been shown that even the bulk NMR properties of these materials can provide crucial insight. For example, the real-space signature of band inversion can be seen as a charge re-distribution between

different crystal sites. Hence, NMR together with DFT can be used to identify, e.g.,  $\text{Bi}_2\text{Se}_3$  as a topological insulator already from its bulk properties. [22].

Unfortunately, for the time being it is difficult to find universal signatures, considering that the real NMR results depend crucially on the material under study and are often contradictory. For example, in our  $\text{ZrOsSi}$  case,  $T_1$  values are longer and shifts are positive compared to their metallic counterparts,  $\text{TaOsSi}$  and  $\text{NbOsSi}$ . However, these are exactly opposite to the  $^{209}\text{Bi}$  NMR results in  $\text{YPdBi}$  and  $\text{YPtBi}$ , where the authors conclude that “it seems plausible that short  $T_1$  values and negative shifts are universal features of the band inversion in topologically nontrivial materials” [21]. From the above discussion, it is clear that, while NMR is able to distinguish topological nontrivial materials from their standard counterparts, such signature is far from universal and of not an easy interpretation.

## 4 CONCLUSION

$(\text{Ta}, \text{Nb}, \text{Zr})\text{OsSi}$  are topological semimetals whose crystal structure has a very low degree of symmetry. As a result, they provide a unique opportunity to identify the nature of their different electronic phases based on symmetry considerations alone. For example, the time-reversal symmetry (TRS) breaking superconducting states stabilized in  $(\text{Ta}, \text{Nb})\text{OsSi}$  can be identified as nonunitary triplet types. The nonsymmorphic glide mirror symmetries of the  $Pnma$  space group play an important role in determining the topological properties of  $(\text{Ta}, \text{Nb})\text{OsSi}$ . While  $(\text{Ta}, \text{Nb})\text{OsSi}$  are nonsymmorphic symmetry-protected semimetals [11, 12, 13, 14],  $\text{ZrOsSi}$  is a  $Z_2$  topological metal. As a result,  $\text{ZrOsSi}$  is expected to realize ordered phases that are *qualitatively different* from those of  $(\text{Ta}, \text{Nb})\text{OsSi}$ .  $\text{ZrOsSi}$  also superconducts [15], but its transition temperature,  $T_c \sim 1.7$  K, is much lower than  $T_c \sim 5.5$  K of  $\text{TaOsSi}$  and  $T_c \sim 3.1$  K of  $\text{NbOsSi}$  [14]. Given that the superconducting ground states of  $(\text{Ta}, \text{Nb})\text{OsSi}$  break TRS, it would be interesting to look for TRS-breaking superconductivity in  $\text{ZrOsSi}$ . Most importantly, since  $\text{ZrOsSi}$  is similar to a doped topological insulator [35], it could act as a platform for realizing a novel topological superconducting ground state. In addition, unlike  $(\text{Cs}, \text{Rb}, \text{K})\text{V}_3\text{Sb}_5$  [9],  $\text{ZrOsSi}$  does not bring the complications arising from inherent geometric frustration of crystal structure. This makes it a very attractive candidate for studying the interplay between topology and electronic correlations.

In summary, from detailed DFT band-structure calculations combined with extensive NMR measurements, we show that replacing Ta or Nb in  $(\text{Ta}, \text{Nb})\text{OsSi}$  with Zr, modifies qualitatively the properties of the compound. We prove that, although all of them are superconductors,  $(\text{Ta}, \text{Nb})\text{OsSi}$  are very good metals, while  $\text{ZrOsSi}$  exhibits features of a doped strong topological insulator. In general, since all the three materials are topologically nontrivial and superconduct at ambient pressure, they provide possible candidate platforms for realizing topological superconductivity in stoichiometric materials. Our results further confirm that the combination of DFT and NMR is a powerful tool to investigate the topological properties of quantum materials.

## DATA AVAILABILITY STATEMENT

The raw data supporting the conclusions of this article can be made available by the authors upon reasonable request.

## AUTHOR CONTRIBUTIONS

XX and TS initiated, designed, and supervised the project. SKG and BL performed the electronic band-structure calculations. CX and XX synthesized and characterized the samples. ADH and PKB discussed the results. SKG and TS wrote the manuscript to which all co-authors contributed.

## FUNDING

SKG acknowledges the Indian Institute of Technology, Kanpur for the financial support through the Initiation Grant (IITK/PHY/2022116). XX acknowledges the financial support from the National Natural Science Foundation of China under Grant nos. 11974061 and 12274369. This work was financially supported in part by the Schweizerische Nationalfonds zur Förderung der Wissenschaftlichen Forschung (SNF), Grant no. 200021-169455.

## ACKNOWLEDGMENTS

The authors acknowledge T. Tula and J. Quintanilla for enlightening discussions.

## CONFLICT OF INTEREST STATEMENT

The authors declare that the research was conducted in the absence of any commercial or financial relationships that could be construed as a potential conflict of interest.

## REFERENCES

- [1] Armitage NP, Mele EJ, Vishwanath A. Weyl and Dirac semimetals in three-dimensional solids. *Rev. Mod. Phys.* **90** (2018) 015001.
- [2] Lv BQ, Qian T, Ding H. Experimental perspective on three-dimensional topological semimetals. *Rev. Mod. Phys.* **93** (2021) 025002.
- [3] Ortiz BR, Teicher SML, Hu Y, Zuo JL, Sarte PM, Schueller EC, et al. CsV<sub>3</sub>Sb<sub>5</sub>: A Z<sub>2</sub> topological kagome metal with a superconducting ground state. *Phys. Rev. Lett.* **125** (2020) 247002.
- [4] Sakano M, Okawa K, Kanou M, Sanjo H, Okuda T, Sasagawa T, et al. Topologically protected surface states in a centrosymmetric superconductor  $\beta$ -PdBi<sub>2</sub>. *Nat. Commun.* **6** (2015) 1–7.
- [5] Ghosh SK, Smidman M, Shang T, Annett JF, Hillier AD, Quintanilla J, et al. Recent progress on superconductors with time-reversal symmetry breaking. *J. Phys. Condens. Matter* **33** (2020) 033001.
- [6] Shang T, Ghosh SK, Smidman M, Gawryluk DJ, Baines C, Wang A, et al. Spin-triplet superconductivity in Weyl nodal-line semimetals. *npj Quantum Mater.* **7** (2022) 1–9.
- [7] Badger JR, Quan Y, Staab MC, Sumita S, Rossi A, Devlin KP, et al. Dirac lines and loop at the Fermi level in the time-reversal symmetry breaking superconductor LaNiGa<sub>2</sub>. *Commun. Phys.* **5** (2022) 22.
- [8] Ghosh SK, Csire G, Whittlesea P, Annett JF, Gradhand M, Újfalussy B, et al. Quantitative theory of triplet pairing in the unconventional superconductor LaNiGa<sub>2</sub>. *Phys. Rev. B* **101** (2020) 100506.
- [9] Neupert T, Denner MM, Yin JX, Thomale R, Hasan MZ. Charge order and superconductivity in kagome materials. *Nat. Phys.* **18** (2022) 137–143.
- [10] Jiang K, Wu T, Yin JX, Wang Z, Hasan MZ, Wilson SD, et al. Kagome superconductors AV<sub>3</sub>Sb<sub>5</sub> (A = K, Rb, Cs). *Natl. Sci. Rev.* **9** (2022) nwac199.
- [11] Wang Z, Alexandradinata A, Cava RJ, Bernevig BA. Hourglass fermions. *Nature* **532** (2016) 189–194.

- [12] Li S, Liu Y, Wang SS, Yu ZM, Guan S, Sheng XL, et al. Nonsymmorphic-symmetry-protected hourglass Dirac loop, nodal line, and Dirac point in bulk and monolayer  $X_3\text{SiTe}_6$  ( $X = \text{Ta}, \text{Nb}$ ). *Phys. Rev. B* **97** (2018) 045131.
- [13] Cuono G, Forte F, Cuoco M, Islam R, Luo J, Noce C, et al. Multiple band crossings and Fermi surface topology: Role of double nonsymmorphic symmetries in MnP-type crystal structures. *Phys. Rev. Mater.* **3** (2019) 095004.
- [14] Ghosh SK, Biswas PK, Xu C, Li B, Zhao JZ, Hillier AD, et al. Time-reversal symmetry breaking superconductivity in three-dimensional Dirac semimetallic silicides. *Phys. Rev. Res.* **4** (2022) L012031.
- [15] Benndorf C, Heletta L, Heymann G, Huppertz H, Eckert H, Pöttgen R. NbOsSi and TaOsSi — Two new superconducting ternary osmium silicides. *Solid State Sci.* **68** (2017) 32–38.
- [16] Hasan MZ, Kane CL. Colloquium: Topological insulators. *Rev. Mod. Phys.* **82** (2010) 3045–3067.
- [17] Wu S, Fatemi V, Gibson QD, Watanabe K, Taniguchi T, Cava RJ, et al. Observation of the quantum spin Hall effect up to 100 kelvin in a monolayer crystal. *Science* **359** (2018) 76–79.
- [18] Frolov SM, Manfra MJ, Sau JD. Topological superconductivity in hybrid devices. *Nat. Phys.* **16** (2020) 718–724.
- [19] Browne AJ, Krajewska A, Gibbs AS. Quantum materials with strong spin-orbit coupling: challenges and opportunities for materials chemists. *J. Mater. Chem. C* **9** (2021) 11640–11654.
- [20] Massiot D, Messinger RJ, Cadars S, Deschamps M, Montouillout V, Pellerin N, et al. Topological, geometric, and chemical order in materials: insights from solid-state NMR. *Acc. Chem. Res.* **46** (2013) 1975–1984.
- [21] Nowak B, Kaczorowski D. NMR as a probe of band inversion in topologically nontrivial half-Heusler compounds. *J. Phys. Chem. C* **118** (2014) 18021–18026.
- [22] Nachtigal J, Chong SV, Williams GVM, Isaeva A, Oeckler O, Haase J, et al.  $^{125}\text{Te}$  NMR study of the bulk of topological insulators  $\text{Bi}_2\text{Te}_3$  and  $\text{Sb}_2\text{Te}_3$ . *Z. Anorg. Allg. Chem.* **648** (2022) e202200208.
- [23] Nisson DM, Curro NJ. Nuclear magnetic resonance Knight shifts in the presence of strong spin-orbit and crystal-field potentials. *New J. Phys.* **18** (2016) 073041.
- [24] Boutin S, Ramírez-Ruiz J, Garate I. Tight-binding theory of NMR shifts in topological insulators  $\text{Bi}_2\text{Se}_3$  and  $\text{Bi}_2\text{Te}_3$ . *Phys. Rev. B* **94** (2016) 115204.
- [25] Zhang X, Hou Z, Wang Y, Xu G, Shi C, Liu E, et al. NMR evidence for the topologically nontrivial nature in a family of half-Heusler compounds. *Sci. Rep.* **6** (2016) 1–7.
- [26] Young BL, Lai ZY, Xu Z, Yang A, Gu GD, Pan ZH, et al. Probing the bulk electronic states of  $\text{Bi}_2\text{Se}_3$  using nuclear magnetic resonance. *Phys. Rev. B* **86** (2012) 075137.
- [27] Koumoulis D, Chasapis TC, Taylor RE, Lake MP, King D, Jarenwattananon NN, et al. NMR probe of metallic states in nanoscale topological insulators. *Phys. Rev. Lett.* **110** (2013) 026602.
- [28] Choi DM, Lee CE.  $^{77}\text{Se}$  nuclear magnetic resonance study of the surface effect in topological insulator  $\text{Bi}_2\text{Se}_3$  nanoparticles. *J. Korean Phys. Soc.* **72** (2018) 835–837.
- [29] Papawassiliou W, Jaworski A, Pell AJ, Jang JH, Kim Y, Lee SC, et al. Resolving Dirac electrons with broadband high-resolution NMR. *Nat. Commun.* **11** (2020) 1–7.
- [30] Park JK, Kwon HJ, Lee CE. NMR observation of mobile protons in proton-implanted ZnO nanorods. *Sci. Rep.* **6** (2016) 1–8.
- [31] Hoch MJR, Holcomb DF.  $^{31}\text{P}$  Knight shifts and spin dynamics in Si:P at temperatures comparable to the Fermi temperature. *Phys. Rev. B* **71** (2005) 035115.
- [32] Tian Y, Ghassemi N, Ross JH. Dirac electron behavior and NMR evidence for topological band inversion in  $\text{ZrTe}_5$ . *Phys. Rev. B* **100** (2019) 165149.
- [33] Guehne R, Haase J, Shekhar C, Felser C. Field-induced charge symmetry revealed by nuclear magnetic resonance in the topological insulator  $\text{Bi}_2\text{Te}_3$ . *Phys. Rev. Res.* **3** (2021) L012018.
- [34] Dioguardi AP, Yasuoka H, Thomas SM, Sakai H, Cary SK, Kozimor SA, et al.  $^{239}\text{Pu}$  nuclear magnetic resonance in the candidate topological insulator  $\text{PuB}_4$ . *Phys. Rev. B* **99** (2019) 035104.

- [35] Sato M, Ando Y. Topological superconductors: a review. *Rep. Prog. Phys.* **80** (2017) 076501.
- [36] Xu CQ, Li B, Feng JJ, Jiao WH, Li YK, Liu SW, et al. Two-gap superconductivity and topological surface states in TaOsSi. *Phys. Rev. B* **100** (2019) 134503.
- [37] Blaha P, Schwarz K, Tran F, Laskowski R, Madsen GKH, Marks LD. WIEN2k: An APW+lo program for calculating the properties of solids. *J. Chem. Phys.* **152** (2020) 074101.
- [38] Perdew JP, Burke K, Ernzerhof M. Generalized Gradient Approximation Made Simple. *Phys. Rev. Lett.* **77** (1996) 3865.
- [39] Campbell D, Collini J, Sławińska J, Autieri C, Wang L, Wang K, et al. Topologically driven linear magnetoresistance in helimagnetic FeP. *npj Quantum Mater.* **6** (2021) 38.
- [40] Fu L, Kane CL. Topological insulators with inversion symmetry. *Phys. Rev. B* **76** (2007) 045302.
- [41] Soluyanov AA, Vanderbilt D. Computing topological invariants without inversion symmetry. *Phys. Rev. B* **83** (2011) 235401.
- [42] Wu Q, Zhang S, Song HF, Troyer M, Soluyanov AA. WannierTools: An open-source software package for novel topological materials. *Comput. Phys. Commun.* **224** (2018) 405–416.
- [43] Marsmann HC. <sup>29</sup>Si NMR. Lindon JC, editor, *Encyclopedia of Spectroscopy and Spectrometry* (Oxford: Elsevier) (1999), 2031–2042.
- [44] Korringa J. Nuclear magnetic relaxation and resonance line shift in metals. *Physica* **16** (1950) 601–610.
- [45] Herman F, Kuglin CD, Cuff KF, Kortum RL. Relativistic corrections to the band structure of tetrahedrally bonded semiconductors. *Phys. Rev. Lett.* **11** (1963) 541–545.
- [46] Herman F, Skillman S. *Atomic Structure Calculations* (Englewood Cliffs, N.J.: Prentice Hall) (1963).
- [47] Shanavas KV, Popović ZS, Satpathy S. Theoretical model for Rashba spin-orbit interaction in *d* electrons. *Phys. Rev. B* **90** (2014) 165108.
- [48] Cordero B, Gómez V, Platero-Prats AE, Revcoécs M, Echeverría J, Cremades E, et al. Covalent radii revisited. *Dalton Trans.* **21** (2008) 2832.
- [49] Hebel LC, Slichter CP. Nuclear spin relaxation in normal and superconducting aluminum. *Phys. Rev.* **113** (1959) 1504–1519.
- [50] Weger M. NMR in superconductors. *Pure Appl. Chem.* **32** (1972) 325–338.
- [51] MacLaughlin DE. Magnetic resonance in the superconducting state. Ehrenreich H, Seitz F, Turnbull D, editors, *Solid State Physics* (San Diego: Academic Press), vol. 31 (1976), 1–69. And references therein.

